

# Determination of Hund's coupling in 5d Oxides using Resonant Inelastic X-ray Scattering

Bo Yuan,<sup>1</sup> J. P. Clancy,<sup>1</sup> A. M. Cook,<sup>1,2</sup> C. M. Thompson,<sup>3,\*</sup> J. Greedan,<sup>3,4</sup> G. Cao,<sup>5</sup> B. C. Jeon,<sup>6,7</sup> T. W. Noh,<sup>6,7</sup> M. H. Upton,<sup>8</sup> D. Casa,<sup>8</sup> T. Gog,<sup>8</sup> A. Paramakanti,<sup>1</sup> and Young-June Kim<sup>1,†</sup>

<sup>1</sup>*Department of Physics, University of Toronto, Toronto, Ontario M5S 1A7, Canada*

<sup>2</sup>*Department of Physics, University of Zurich, Winterthurerstrasse 190, 8057 Zurich, Switzerland*

<sup>3</sup>*Department of Chemistry and Chemical Biology,*

*McMaster University, Hamilton, Ontario L8S 4L8, Canada*

<sup>4</sup>*Brockhouse Institute for Materials Research, McMaster University, Hamilton, Ontario L8S 4L8, Canada*

<sup>5</sup>*Department of Physics, University of Colorado-Boulder, Boulder, Colorado 80309, USA*

<sup>6</sup>*Center for Correlated Electron Systems, Institute for Basic Science (IBS), Seoul 08826, Republic of Korea*

<sup>7</sup>*Department of Physics & Astronomy, Seoul National University, Seoul 08826, Republic of Korea*

<sup>8</sup>*XOR, Advanced Photon Source, Argonne National Laboratory, Argonne, Illinois 60439, USA*

(Dated: July 1, 2021)

We report resonant inelastic X-ray scattering (RIXS) measurements on ordered double perovskite samples containing  $\text{Re}^{5+}$  and  $\text{Ir}^{5+}$  with  $5d^2$  and  $5d^4$  electronic configurations respectively. In particular, the observed RIXS spectra of  $\text{Ba}_2\text{YReO}_6$  and  $\text{Sr}_2\text{MfIrO}_6$  ( $\text{M}=\text{Y}, \text{Gd}$ ) show sharp intra- $t_{2g}$  transitions, which can be quantitatively understood using a minimal ‘atomic’ Hamiltonian incorporating spin-orbit coupling ( $\lambda$ ) and Hund's coupling ( $J_H$ ). Our analysis yields  $\lambda = 0.38(2)\text{eV}$  with  $J_H = 0.26(2)\text{eV}$  for  $\text{Re}^{5+}$ , and  $\lambda = 0.42(2)\text{eV}$  with  $J_H = 0.25(4)\text{eV}$  for  $\text{Ir}^{5+}$ . Our results provide the first sharp estimates for the Hund's coupling in 5d oxides, and suggest that it should be treated on equal footing with spin-orbit interaction in multi-orbital 5d transition metal compounds.

PACS numbers:

## I. INTRODUCTION

Hund's coupling,  $J_H$ , represents the local spin exchange interaction for electrons in multiorbital systems, and it is responsible for a variety of interesting phenomena in solids. For example, Hund's coupling is responsible for spin-state transitions as a function of temperature in certain insulating 3d transition metal compounds<sup>1–5</sup>. More remarkably, Hund's coupling has two distinct and contrary effects in multiband metals<sup>6</sup>. On the one hand, it suppresses the atomic charge gap, making it energetically unfavorable for electrons to be localized and become a Mott insulator. On the other hand, it promotes strongly correlated bad-metal behavior by rendering Fermi liquid quasiparticles incoherent. This dichotomous role played by  $J_H$  is now recognized to be important in the widely studied iron pnictides<sup>7–13</sup>, as well as in ruthenates like  $\text{Ca}_2\text{RuO}_4$ <sup>14,15</sup>.

In recent years, there has been an increasing interest in complex 5d oxides. In these systems, there is an intricate interplay of electronic correlation, Hund's coupling, spin-orbit coupling (SOC)  $\lambda$ , and electron kinetic energy, which leads to novel ground states<sup>16</sup>. This underscores the need to accurately determine these energy scales, which has important ramifications for magnetism, bad metal behavior, and Mott transitions in 5d oxides. For example, density functional theory calculations predict the honeycomb material  $(\text{Na},\text{Li})_2\text{IrO}_3$  to exhibit a large bandwidth and weakly correlated behavior<sup>17,18</sup>. However, experiments show that it is better described as a  $J_{\text{eff}} = 1/2$  Mott insulator<sup>19–21</sup>, in agreement with a recent exact diagonalization study which accounts for

local correlation effects<sup>22</sup>. Similarly,  $d^4$  systems with strong SOC have been predicted to behave as localized  $J_{\text{eff}} = 0$  insulators, with magnetism induced by exciton condensation<sup>23–26</sup> or impurity effects<sup>27</sup>, while band theory<sup>28</sup> provides an itinerant magnetism explanation for the observed Ir magnetic moment in  $\text{A}_2\text{YIrO}_6$  ( $\text{A}=\text{Ba},\text{Sr}$ )<sup>27,29</sup>. Incorporation of correlation effects appear to be necessary to resolve the controversy in understanding magnetism in  $d^4$  double perovskites. The interplay of SOC and Hund's coupling is also clearly important in understanding the electronic ground states in multi-electron  $5d^2$  rhenates and  $5d^3$  osmates<sup>30,31</sup>. While Hund's coupling is irrelevant for the single-hole atomic configuration of Mott insulating  $5d^5$  iridates, it is important for superexchange processes which involve intermediate  $5d^4$  configurations (two-hole states). This determines the strength of the conventional Heisenberg interaction relative to the unconventional Kitaev exchange which can drive an exotic quantum spin liquid in honeycomb-based materials<sup>20,21,32–40</sup>.

Remarkably, despite this wide interest in complex 5d oxides and the importance of the Hund's coupling for understanding their magnetic properties, there has been no direct and accurate experimental determination of  $J_H$  in these systems. The values for  $J_H$  used in numerical calculations on 5d oxides vary widely, ranging from  $J_H = 0.2\text{eV}$  to  $0.6\text{eV}$ <sup>18,22,27,41,42</sup>, while analytical studies typically focus on the simple limits  $J_H \gg \lambda$  or  $J_H \ll \lambda$ .

In this paper, we use resonant inelastic X-ray scattering (RIXS) to explore local spin-orbital excitations in  $\text{Ir}^{5+}$  ( $5d^4$ ) and  $\text{Re}^{5+}$  ( $5d^2$ ) double perovskites. Use of the two complementary 5d insulating oxides modeled by

an effective ‘atomic’ Hamiltonian allows us to determine these important energy scales,  $J_H$  and  $\lambda$  with high precision. We find  $\lambda(\text{Ir})=0.42(2)\text{eV}$  with  $J_H(\text{Ir})=0.25(4)\text{eV}$ , and  $\lambda(\text{Re})=0.38(2)\text{eV}$  with  $J_H(\text{Re})=0.26(2)\text{eV}$ . The  $J_H$  values obtained here represent the first measurements for rhenates and iridates.

## II. EXPERIMENTAL METHODS

In our study, we choose to work with ordered double perovskite (DP) compounds  $\text{A}_2\text{BB}'\text{O}_6$  ( $\text{B}=\text{Ir}, \text{Re}$ ) which offer two distinct advantages. In  $\text{Ba}_2\text{YReO}_6$  and  $\text{Sr}_2\text{YIrO}_6$ , the Re/Ir octahedra form a rock-salt structure with adjacent octahedra centered around inert  $\text{Y}^{3+}$  ions. The intervening electronically inactive  $\text{YO}_6$  octahedra ensures that the overlap between the neighboring Re/Ir orbitals is small, leading to extremely narrow spectral bandwidths as shown in our RIXS data. This allows us to focus on the local physics, and justifies our use of an ‘atomic’ Hamiltonian to model the data. The second benefit of using DPs has to do with suppression of the Jahn-Teller (J-T) instability. In a perovskite structure with octahedra formed by  $d^2$  or  $d^4$  ions, there is a tendency for a cooperative J-T effect, in which neighboring octahedra distort in a complementary manner which strongly breaks the local octahedral symmetry. However, if the J-T active octahedron is surrounded by octahedra containing non-J-T ions (such as  $\text{Fe}^{3+}$  or  $\text{Y}^{3+}$ ), this instability is suppressed<sup>43</sup>. As a result, although the  $\text{ReO}_6$  and  $\text{IrO}_6$  octahedra in the DP structure may undergo small rotations, they lead to very weak deviations from an ideal local octahedral environment.

Two different experimental setups were used for the RIXS experiments at the Advanced Photon Source. For the Ir  $L_3$  (Re  $L_2$ ) edge RIXS experiments carried out at the 9ID (27ID) beamline, the beam was monochromatized by Si(844) [Si(400)] crystals. A spherical (1-m-radius) diced Si(844) [Si(773)] analyzer was used to select final photon energy. In order to minimize the elastic background intensity, measurements were carried out in a horizontal scattering geometry, for which the scattering angle  $2\theta$  was close to 90 degrees. The overall energy resolution of about 40 meV (FWHM) for Ir and 100 meV for Re was obtained. The Re-DP samples used in our measurements,  $\text{Ba}_2\text{YReO}_6$ ,  $\text{Ba}_2\text{FeReO}_6$ , and  $\text{Ca}_2\text{FeReO}_6$ , were all polycrystalline powder samples pressed into pellets. For Ir-DP measurements, we used single crystals of  $\text{Sr}_2\text{YIrO}_6$  and  $\text{Sr}_2\text{GdIrO}_6$ . The synthesis and characterization of these samples have been previously reported<sup>29,44–48</sup>, and all samples show high degree of B/B’ order due to the valence difference.

## III. EXPERIMENTAL RESULTS

Incident energy ( $E_i$ ) dependence of  $\text{Ba}_2\text{YReO}_6$  RIXS spectra are shown in Fig. 1. One can resolve three main

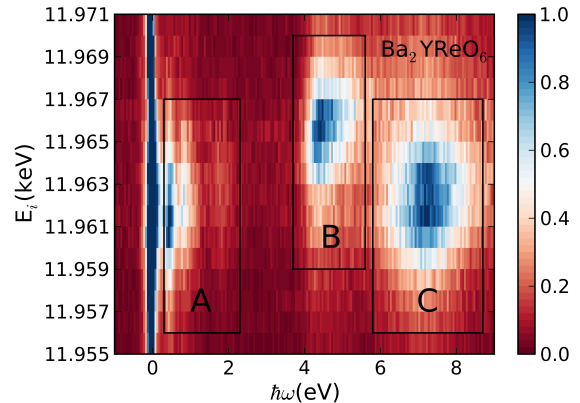


FIG. 1: Incident energy ( $E_i$ ) dependence of  $\text{Ba}_2\text{YReO}_6$  RIXS spectra. The RIXS intensity is plotted as a function of incident energy  $E_i$  (vertical axis) and energy transfer  $\hbar\omega$  (horizontal axis). An arbitrary intensity scale is used where blue (red) denotes higher(lower) intensity.

features with  $\hbar\omega \lesssim 2.5\text{eV}$  (feature A),  $4\text{eV} \lesssim \hbar\omega \lesssim 6\text{eV}$  (feature B) and  $6\text{eV} \lesssim \hbar\omega \lesssim 8\text{eV}$  (feature C). Both features A and C show enhancement when  $E_i$  is tuned near the resonance energy of  $E_i \approx 11.961\text{keV}$ , whereas feature B resonates at slightly higher  $E_i \approx 11.965\text{keV}$ . RIXS follows a second order process (dipole transition from  $2p$  to  $5d$  and another transition back to  $2p$ ) with an intermediate state consisting of a  $2p$  core hole and an excited electron in either  $t_{2g}$  or  $e_g$  states. Different resonant energies thus reflect different intermediate states in these transitions. This allows us to assign A and C as intra  $t_{2g}$  and charge transfer (CT) excitation from the surrounding ligands to  $t_{2g}$  states, respectively, and B as  $t_{2g} - e_g$  transition. The intermediate states of both intra- $t_{2g}$  and CT excitation are  $\underline{2pt}_{2g}^3$ , where the underline denotes a  $2p$  core-hole. On the other hand, the intermediate state for  $t_{2g} - e_g$  transition is  $\underline{2pt}_{2g}^2 e_g^1$ , which occurs at higher energy than  $\underline{2pt}_{2g}^3$ . The difference in resonant energies thus corresponds to the  $t_{2g} - e_g$  splitting. As discussed earlier, the spatial extent of the  $5d$  orbital leads to a large  $t_{2g}-e_g$  splitting, while the  $t_{2g}$  orbitals are further split by  $J_H$  and  $\lambda$  as shown in the figure. We note that strong fluorescence features were observed around 10 eV in the study of metallic rhenate samples  $\text{ReO}_2$  and  $\text{ReO}_3$ <sup>49</sup>, which is absent in our  $E_i$ -dependence study of insulating  $\text{Ba}_2\text{YReO}_6$ . Qualitatively similar incident energy dependence has been reported for iridate samples in the past<sup>50</sup>

Room temperature RIXS spectra of all DP samples are shown in Fig. 2. Wide-range scans are shown in insets of panels (a) and (b), for Ir-DP and Re-DP, respectively. The low-energy region below 2.5eV are zoomed in and shown in the main panels. All samples are found to exhibit qualitatively similar excitation spectra: a set of sharp peaks in the low energy range  $\lesssim 2.5\text{eV}$  (the sharp  $\hbar\omega = 0$  peaks are due to elastic background and repre-

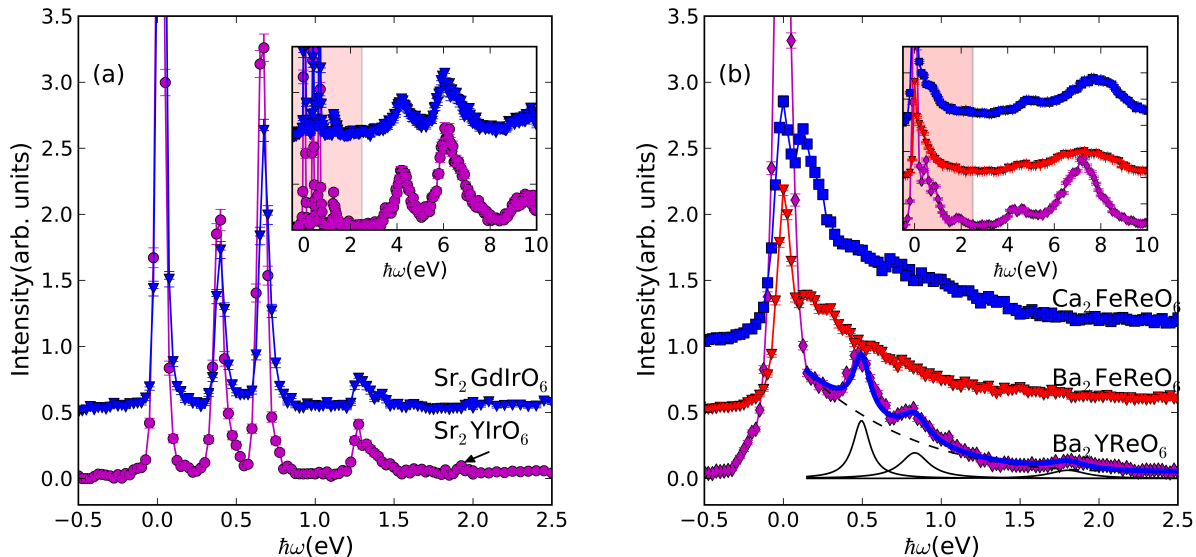


FIG. 2: RIXS spectra of (a) Ir double perovskites and (b) Re double perovskites. Main panels show details of intra- $t_{2g}$  excitations in the energy range  $\hbar\omega < 2.5\text{eV}$ , while full RIXS spectra covering wide range of energy transfer  $\hbar\omega < 10\text{eV}$  are shown in insets. Incident energy  $E_i=11.215\text{keV}$  and  $E_i=11.961\text{keV}$  with fixed  $Q$  near  $2\theta = 90^\circ$  were used to obtain spectra in (a) and (b) respectively. The scans are vertically offset for visual clarity, and the intensity scale is arbitrary. The arrow in (a) indicates the weak  $\sim 2\text{eV}$  feature (see text). The thick blue line in (b) is a fit to the  $\text{Ba}_2\text{YReO}_6$  spectrum as described in the text. Contributions from individual peaks are shown as black solid lines. Dashed line indicates the sloping quartic background.

sent instrumental resolution), and two broader peaks in the high energy 4-8eV range. Despite the similarity in the peak positions, we find a systematic difference in the peak widths when comparing different samples. In particular, metallic  $\text{Ba}_2\text{FeReO}_6$  and semimetallic  $\text{Ca}_2\text{FeReO}_6$  exhibit very broad features, clearly contrasting the other (insulating) samples, which exhibit well-resolved peaks. We thus focus below on the spectra of only the insulating samples in order to extract quantitative information from the peak positions.

As shown in Fig. 2 (a), the Ir-DP samples display sharp features that are resolution limited. The three inelastic peak positions in both  $\text{Sr}_2\text{GdIrO}_6$  and  $\text{Sr}_2\text{YIrO}_6$  can be read directly from their spectra:  $0.39(2)\text{eV}$ ,  $0.66(2)\text{eV}$ , and  $1.30(6)\text{eV}$ . No momentum dependence was found for these features (See Appendix). In addition, there is a very weak feature at  $\sim 2\text{eV}$  in both iridates. We note that the crystal structure of these two compounds are different;  $\text{Sr}_2\text{YIrO}_6$  and  $\text{Sr}_2\text{GdIrO}_6$  crystallize, respectively, in monoclinic and cubic symmetry<sup>29</sup>. In addition, the  $\text{IrO}_6$  octahedra are slightly flattened along the apical direction in  $\text{Sr}_2\text{YIrO}_6$ , with distinct Ir-O bond lengths  $1.9366\text{\AA}$  (apical),  $1.9798\text{\AA}$ , and  $1.9723\text{\AA}$ . However, the octahedra in  $\text{Sr}_2\text{GdIrO}_6$  are almost undistorted<sup>29</sup>. The lack of momentum dependence of the inelastic features and the fact that we observe almost the same peak positions in these two systems suggest that the electronic structure is determined by local physics such as  $\lambda$  and  $J_H$ , and is unaffected by the global symmetry or the presence

of a small distortion.

In contrast to the Ir-DPs, the spectral features in the Re-DPs are much broader, partly because of coarser energy resolution. In addition, metallic samples are expected to exhibit large peak width resulting from stronger damping due to particle-hole continuum as well as powder averaging effect, as is seen for  $\text{Ba}_2\text{FeReO}_6$  and  $\text{Ca}_2\text{FeReO}_6$ . However, for insulating  $\text{Ba}_2\text{YReO}_6$ , we find three peaks that can be clearly resolved on top of a broad continuum, so we focus on only this rhenate in our analysis below. The low energy continuum is modeled with a quartic background - as discussed later, we tentatively attribute this background to coupled multiphonon/magnon contributions. To extract peak positions, the low energy spectrum from 0.15-2.5eV is fitted with 3 Lorentzians as shown in Fig. 2(b). From these fits, we extract peak positions  $0.49(3)\text{eV}$ ,  $0.83(4)\text{eV}$  and  $1.85(5)\text{eV}$ . The corresponding FWHM are  $0.13(4)\text{eV}$ ,  $0.22(8)\text{eV}$ , and  $0.29(8)\text{eV}$ , respectively.

#### IV. THEORETICAL MODEL

We next turn to a theoretical modelling of our data. We begin by noting that the sharp, momentum-independent, inelastic peaks found in our RIXS measurements suggest that a local Hamiltonian is appropriate for understanding these excitations. Furthermore, the two sets of compounds in our RIXS study are particle-

hole conjugates, with the rhenates being at a filling of 2-electrons while the iridates are at a filling of 2-holes. While the local atomic interactions are particle-hole symmetric, SOC breaks this symmetry. As a result, projecting to the  $t_{2g}$  orbitals, both sets of materials can be described by the same Kanamori Hamiltonian,

$$H_{\text{eff}} = -2J_H \vec{S}^2 - \frac{J_H}{2} \vec{L}^2 \pm \lambda(\vec{l}_1 \cdot \vec{s}_1 + \vec{l}_2 \cdot \vec{s}_2) \quad (1)$$

where  $+$ ( $-$ ) with the 2-hole (2-electron) picture applies for the  $d^4$ ( $d^2$ ) configuration, and  $\vec{L}$  and  $\vec{S}$  refer to the total orbital and spin angular momenta respectively of the two particles. For  $J_H \ll \lambda$ , the eigenstates are obtained by perturbing around the noninteracting limit which corresponds to occupying the  $j_{\text{eff}} = 1/2$  and  $j_{\text{eff}} = 3/2$  multiplets arising from SOC<sup>51</sup>. For large  $J_H$ , the eigenstates should be understood as arising from  $\vec{S}$  and  $\vec{L}$  being locked together by SOC. In either limit, the  $d^2$  ( $d^4$ ) case exhibits a ground state with  $J_{\text{eff}} = 2$  ( $J_{\text{eff}} = 0$ ). The  $d^2$  vs  $d^4$  difference arises due to the opposite signs of the effective SOC. While we expect  $J_H$  and  $\lambda$  to be similar for Ir and Re, we do not demand that they be identical.

To extract  $\lambda$  and  $J_H$ , we plot the calculated excitation energies for the two cases (Ir and Re) as a function of  $J_H/\lambda$  for different choices of  $\lambda$ , as shown in Fig. 3, and superpose on this the observed peak positions. For the correct choice of  $\lambda$ , the computed curves should intersect *all* the observed peaks at a *common* value of  $J_H/\lambda$ , allowing us to extract both  $\lambda$  and  $J_H/\lambda$ .

Figs. 3(a-c) show the theoretically computed spectra for the Ir-DPs as a function of  $J_H/\lambda$  for increasing values of SOC:  $\lambda = 0.39\text{eV}$ ,  $0.42\text{eV}$ , and  $0.45\text{eV}$  respectively. We also show on these plot the three experimentally observed modes as thick colored lines (pink), with the width indicating the experimental uncertainty. For  $\lambda = 0.39\text{eV}$  in Fig. 3(a), we find that the central mode does not intersect the computed spectra for any choice of  $J_H/\lambda$ , while the highest and lowest energy modes intersect for  $0.65 \lesssim J_H/\lambda \lesssim 0.9$  and  $0.45 \lesssim J_H/\lambda \lesssim 0.7$  respectively. For  $\lambda = 0.42\text{eV}$  in Fig. 3(b), we show that there is a range  $0.5 \lesssim J_H/\lambda \lesssim 0.7$ , demarcated by the green shaded region, over which *all* observed modes intersect the theoretical curves. Note that Fig. 3(b) also marks the location of the weak  $\sim 2\text{eV}$  mode with an arrow showing that this also occurs in the correct regime of  $J_H/\lambda$ ; however, given the low intensity of this mode, it should only be viewed as a consistency check. Finally, for even larger SOC,  $\lambda = 0.45\text{eV}$  in Fig. 3(c), we find that while the central mode intersects the computed spectra over a wide range of  $J_H/\lambda$ , the highest and lowest modes now intersect the theoretical curves for nonoverlapping regimes  $J_H/\lambda \lesssim 0.5$  and  $0.7 \lesssim J_H/\lambda \lesssim 1.05$  respectively. Thus, there is no single choice of  $J_H/\lambda$  which would explain all the observed modes for the cases in Fig. 3(a) and (c), while  $\lambda = 0.42\text{eV}$  in Fig. 3(b) is a viable choice for the SOC. We show a similar plot for the Re-DP in Fig. 3(d) for a choice  $\lambda = 0.38\text{eV}$ , where we find a small common intersection window near

$J_H/\lambda \approx 0.7$ . Using this procedure, we conclude that the range of  $\lambda$  values over which such common intersections occur provides an estimate of the SOC, while the window of the common intersection region yields an estimate of  $J_H/\lambda$ . A least squares fit to the peak positions allows us to determine  $J_H$  and  $\lambda$  with remarkably high precision:  $\lambda(\text{Ir}) = 0.42(2)\text{eV}$  with  $J_H(\text{Ir}) = 0.25(4)\text{eV}$ , and  $\lambda(\text{Re}) = 0.38(2)\text{eV}$  with  $J_H(\text{Re}) = 0.26(2)\text{eV}$ . Our result for  $\lambda(\text{Ir})$  is consistent with previous experiments on the single-hole  $5d^5$  iridates<sup>52-55</sup>. Further, since Re ( $Z=75$ ) is close to Ir ( $Z=77$ ) in the periodic table, we expect similar values for  $\lambda$  and  $J_H$ , with a smaller  $\lambda$  for Re given its lower  $Z$ , as is borne out by our analysis. Our work highlights the need to treat  $J_H$  and  $\lambda$  on equal footing in complex  $5d$  oxides.

Interestingly, our model also leads to a simple explanation for why the higher energy peaks in the RIXS data in the 1-2eV range (Fig. 2) have much smaller spectral weight than the two lower energy inelastic peaks. As seen from the theoretical plots in Fig. 3, at  $J_H/\lambda=0$ , the iridates (rhenates) have two sets of excitations, which correspond to exciting one or two holes (electrons) from  $j_{\text{eff}} = 1/2 \rightarrow 3/2$  ( $j_{\text{eff}} = 3/2 \rightarrow 1/2$ ). These occur at excitation energies  $3\lambda/2$  and  $3\lambda$  respectively. However, the latter two-particle excitation is not accessed within the RIXS process at  $J_H/\lambda = 0$ , and thus has *zero* spectral weight. Turning on a small  $J_H > 0$  modifies this result in two important ways: (i) it splits these excitations into multiple branches as seen from Fig. 3, and (ii) it leads to a small nonzero spectral weight  $\sim (J_H/\lambda)^2$  for the higher energy peaks from interaction-induced mixing between the  $j_{\text{eff}}=1/2$  and  $j_{\text{eff}}=3/2$  levels. We have confirmed this picture with a theoretical calculation of the RIXS spectrum for the iridate samples.

## V. THEORETICAL CALCULATION OF RIXS SPECTRUM

The Kramers-Heisenberg expression for the two-photon scattering cross section is given by

$$\frac{d^2\sigma}{d\Omega d\omega} = \frac{\omega'}{\omega} \sum_f \left| \sum_n \frac{\langle f|T^\dagger|n\rangle \langle n|T|i\rangle}{E_i - E_n + \hbar\omega + i\frac{\Gamma_n}{2}} \right|^2 \times \delta(E_i - E_f + \hbar\omega - \hbar\omega'). \quad (2)$$

Here,  $i, n, f$  refer to initial, intermediate, and final states respectively with energies  $E_i, E_n, E_f$ , and  $\Gamma_n$  is the inverse lifetime of the intermediate state with a core-hole.  $\omega, \omega'$  are the incoming and outgoing photon frequencies. The transition is induced by the dipole operator  $T \sim \hat{\epsilon} \cdot \mathbf{r}$ , where  $\hat{\epsilon}$  denotes the photon polarization. Here, we focus on the  $d^4$  iridates at the  $L_3$  resonance within the hole picture, for which the initial and final states come from the two-hole eigenstates on Ir with spin-orbit coupling and Hund's interaction, while the intermediate state corresponds to a single core hole in the atomic  $2P_{3/2}$  manifold

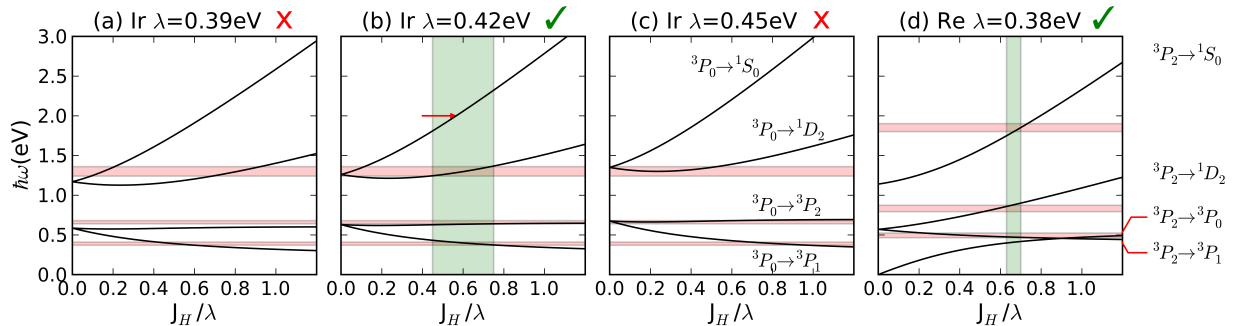


FIG. 3: Calculated excitation energies as a function of  $J_H/\lambda$  are plotted as solid black lines, for Ir (a-c) and Re (d) double perovskites for indicated  $\lambda$  values. Experimentally determined excitation energies (Ir-DP: 0.39(2)eV, 0.66(2)eV, and 1.30(6)eV; Re-DP: 0.49(3)eV, 0.83(4)eV, 1.85(5)eV) are plotted as horizontal colored bands (pink), whose widths reflect the experimental uncertainty. States involved in these transitions are labelled using nomenclature in the  $J_H \gg \lambda$  limit as  $^{2S+1}L_J$ . (a,c) and (b,d) show incorrect and correct choices of  $\lambda$  as described in the text, which are indicated by  $\times$  and  $\checkmark$  respectively. Green shaded regions in (b) and (d) illustrate  $J_H/\lambda$  values for which *all* the observed modes intersect the calculated curves. Red arrow in (b) denotes position of the weak feature  $\sim 2$ eV in the Ir-DPs which would correspond to the highest computed excitation energy.

and a single hole in the  $j_{\text{eff}} = 1/2$  manifold. On resonance, with  $\omega' \approx \omega$  (since the energy transfer is much

smaller than the incoming or outgoing photon energies), the cross section simplifies to

$$\frac{d^2\sigma}{d\Omega d\omega} \approx \left| \frac{1}{E_i - \bar{E}_n + \hbar\omega + i\frac{\bar{\Gamma}_n}{2}} \right|^2 \sum_f \left| \sum_n \langle f|T^\dagger|n\rangle \langle n|T|i\rangle \right|^2 \delta(E_i - E_f + \hbar\omega - \hbar\omega') \quad (3)$$

where  $\bar{E}_n, \bar{\Gamma}_n$  are the average energy and inverse lifetime of the intermediate states.

We can further simplify the transition matrix element as

$$\langle n|T|i\rangle = \epsilon_{\text{in}}^\alpha \langle n|p_{\beta\sigma}^\dagger d_{\alpha\beta\sigma}|i\rangle \quad (4)$$

$$\langle f|T^\dagger|n\rangle = \epsilon_{\text{out}}^\mu \langle f|d_{\mu\nu\sigma'}^\dagger p_{\nu\sigma'}|n\rangle \quad (5)$$

where we have restricted attention to parity-allowed nonzero dipole matrix elements. Here  $p_{\alpha\sigma}^\dagger$  creates a  $2P$  core-hole in orbital  $\alpha$  (i.e.,  $p_x, p_y, p_z$ ) with spin  $\sigma$ , while  $d_{\alpha\beta\sigma}^\dagger$  creates a  $d$ -hole in the  $t_{2g}$  orbital (i.e.,  $d_{yz}, d_{zx}, d_{xy}$ ) with spin  $\sigma$ . Based on the experimental set-up, we fix the incoming polarization to be along the cubic  $x$ -axis, and average the outgoing polarization within the  $yz$  plane since the scattering geometry fixes  $\hat{e}_{\text{in}} \cdot \hat{e}_{\text{out}} = 0$ . Using exact diagonalization for the Hilbert space consisting of 15 states for the two-hole problem with the Hamiltonian in Eq. (1), and the single-hole eigenstates of the  $2P_{3/2}$  and  $j_{\text{eff}} = 1/2$ , we obtain the theoretical RIXS spectrum. Fig. 6 below shows an example of the theoretical spectrum obtained by convolving the above theoretical expression with a Lorentzian resolution function with an experimentally determined width  $\sim 40$ meV, for

a choice  $\lambda = 0.42$ eV and  $J_H = 0.25$ eV. We find that the two lower energy peaks have a strong intensity since they emerge from the allowed single-particle transition across the spin-orbit gap  $3\lambda/2$ , while the two higher energy peaks have a much lower intensity which scales as  $\sim (J_H/\lambda)^2$  for small interactions since they emerge from exciting *two* holes across the spin-orbit gap which is forbidden in the absence of hole-hole interactions arising from Hund's coupling. The resulting spectral intensities are in good agreement with our experimental results.

## VI. DISCUSSION

Despite the excellent agreement between theory and experiments in Fig. 3, there are two unresolved issues. (i) For  $\text{Re}^{5+}$ , the lowest energy peak is expected to be at  $\sim 0.4$ eV. Although this peak is not observed as distinct from the 0.49eV peak in our data, it is possible that there are two nearby peaks which are not resolved in our experiment. (ii) For the Re-DPs, there is considerable spectral weight in the low energy continuum below  $\sim 0.3$  eV. The significant inelastic scattering intensity

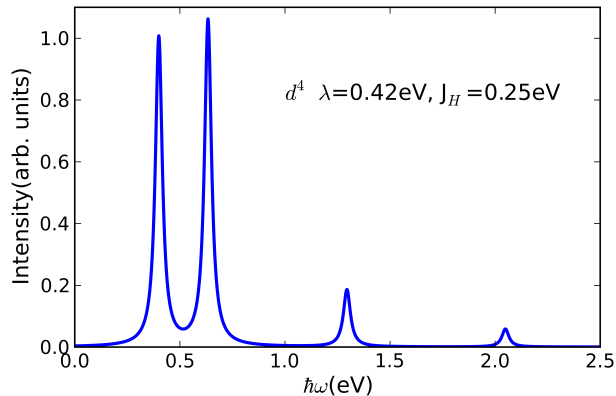


FIG. 4: RIXS spectrum computed for  $d^4$  iridates with  $\lambda = 0.42\text{eV}$ ,  $J_H = 0.25\text{eV}$ .

that was treated as sloping background in our fitting for  $\text{Ba}_2\text{YReO}_6$  (Fig. 2(b)) remains even after subtracting off the non-resonant background (see Appendix). While we can rule out magnon or phonon excitations for energies  $\gtrsim 100\text{meV}$  based on neutron scattering results<sup>56</sup>, multiphonon excitations or some collective excitations of coupled degrees of freedom could exist in this energy range. Future measurements with much higher energy resolution could address these issues.

In conclusion, our RIXS experiments on local spin-orbital excitations in Re and Ir double perovskites, together with a well-justified local model Hamiltonian, allows us to reliably extract the SOC  $\lambda \sim 0.4\text{eV}$  and Hund's coupling  $J_H \sim 0.25\text{eV}$  for rhenates and iridates. We note that a recent study of the  $5d^3$  osmate  $\text{Ba}_2\text{YOsO}_6$  reported a smaller  $\lambda = 0.32(6)\text{eV}$ , and a larger  $J_H = 0.3(2)\text{eV}$ <sup>57</sup>. Although large error bars make these values consistent with our results, it will be interesting to examine whether the discrepancy represents a real difference between  $d^3$  and  $d^2/d^4$  systems. Finally, our results are qualitatively consistent with a  $J_{\text{eff}} = 0$  ( $J_{\text{eff}} = 2$ ) for the ground state of the  $d^4$  iridates ( $d^2$  rhenates); however, our finding that  $J_H < \lambda$  might require revisiting theories of exotic magnetism in  $d^2$  systems based on a strong coupling  $J_H/\lambda \gg 1$  approach<sup>30</sup>.

### Acknowledgments

Research at the University of Toronto was supported by the Natural Sciences and Engineering Research Council of Canada through Discovery Grant. B.Y. would like to acknowledge support from the Canada Graduate Scholarships- Master's Program. B.C.J. and T.W.N. acknowledges the support by IBS-R009-D1. G.C. acknowledges NSF support via grants DMR 1265162 and DMR 1712101. This research used resources of the Advanced Photon Source, a U.S. Department of Energy (DOE) Of-

fice of Science User Facility operated for the DOE Office of Science by Argonne National Laboratory under Contract No. DE-AC02-06CH11357.

### Appendix A: Background subtraction

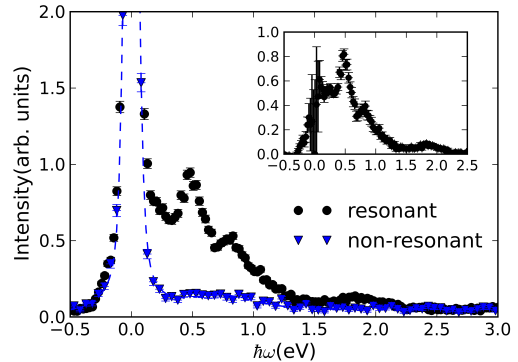


FIG. 5: RIXS spectrum of  $\text{Ba}_2\text{YReO}_6$  at resonant ( $E_i=11.961\text{keV}$ ) and non-resonant incident energy (summed from  $E_i=11.969\text{keV}$  to  $E_i=11.971\text{keV}$ ). The spectra have been scaled to have the same intensity at zero energy transfer. The blue dashed line is fit to the spectrum at non-resonant energy and is used as the background. *Inset*: Inelastic features obtained by subtracting the background off the resonant spectrum. Clear spectral weight is observed for energy transfer  $\hbar\omega < 0.3\text{eV}$ .

Since intensities of the low energy resonant inelastic features are greatly reduced for  $E_i \gtrsim 11.969\text{keV}$ , we can use the spectra in this  $E_i$  range as non-resonant background and subtract from our raw data to study the low energy excitations in  $\text{Ba}_2\text{YReO}_6$ <sup>58</sup>. The non-resonant energy spectrum is obtained by summing over the spectra with  $E_i=11.969\text{keV}$ - $11.971\text{keV}$ , and subtracted off from the spectrum at resonant energy ( $E_i=11.961\text{keV}$ ) as shown in Fig. 5.<sup>58</sup> The background subtracted spectrum shown in Fig. 5 inset clearly reveals the presence of significant spectral weight for  $\hbar\omega \lesssim 0.3\text{eV}$ . This continuum, which exist in *both* metallic  $\text{Ba}_2\text{FeReO}_6$  and insulating  $\text{Ba}_2\text{YReO}_6$ , is not captured in our atomic model, and will require consideration of multiphonon or other collective excitations.

### Appendix B: $\text{Sr}_2\text{YIrO}_6$ : Q-dependence

We show  $\text{Sr}_2\text{YIrO}_6$  RIXS spectra measured at two different Q vectors, separated by approximately a quarter of the Brillouin Zone, in Fig. 6. The inelastic features remain sharp and show no Q dependence, indicating the local nature of these excitations.



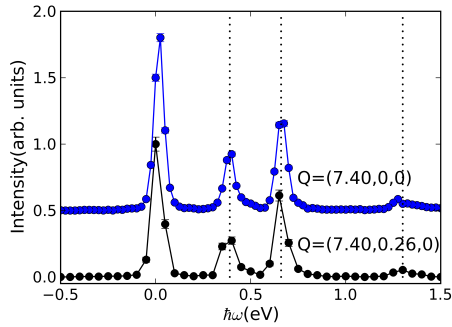


FIG. 6: RIXS spectra of  $\text{Sr}_2\text{YIrO}_6$  at  $\mathbf{Q}=(7.40,0,0)$  and  $\mathbf{Q}=(7.40,0.26,0)$  respectively.  $E_i=11.215\text{keV}$  was used in obtaining both spectra. An arbitrary intensity scale is used and the spectra have been shifted for visual clarity.

- \* Department of Chemistry, Purdue University, 560 Oval Drive, West Lafayette, Indiana 47907-2084, USA
- † Electronic address: yjkim@physics.utoronto.ca
- <sup>1</sup> O. Kahn and C. J. Martinez, *Science* **279**, 44 (1998).
  - <sup>2</sup> R. Heikes, R. Miller, and R. Mazelsky, *Physica* **30**, 1600 (1964).
  - <sup>3</sup> S. Yamaguchi, Y. Okimoto, H. Taniguchi, and Y. Tokura, *Phys. Rev. B* **53**, R2926 (1996).
  - <sup>4</sup> P. G. Radaelli and S.-W. Cheong, *Phys. Rev. B* **66**, 094408 (2002).
  - <sup>5</sup> T. Vogt, P. M. Woodward, P. Karen, B. A. Hunter, P. Henning, and A. R. Moodenbaugh, *Phys. Rev. Lett.* **84**, 2969 (2000).
  - <sup>6</sup> L. de' Medici, J. Mravlje, and A. Georges, *Phys. Rev. Lett.* **107**, 256401 (2011).
  - <sup>7</sup> W. Z. Hu, J. Dong, G. Li, Z. Li, P. Zheng, G. F. Chen, J. L. Luo, and N. L. Wang, *Phys. Rev. Lett.* **101**, 257005 (2008).
  - <sup>8</sup> K. Haule and G. Kotliar, *New J. Phys.* **11**, 025021 (2009).
  - <sup>9</sup> M. D. Johannes and I. I. Mazin, *Phys. Rev. B* **79**, 220510 (2009).
  - <sup>10</sup> W. L. Yang, A. P. Sorini, C.-C. Chen, B. Moritz, W.-S. Lee, F. Vernay, P. Olalde-Velasco, J. D. Denlinger, B. Delley, J.-H. Chu, et al., *Phys. Rev. B* **80**, 014508 (2009).
  - <sup>11</sup> S. Zhou and Z. Wang, *Phys. Rev. Lett.* **105**, 096401 (2010).
  - <sup>12</sup> N. Raghuvanshi and A. Singh, *J. Phys.: Condens. Matter* **23**, 312201 (2011).
  - <sup>13</sup> A. A. Schafgans, S. J. Moon, B. C. Pursley, A. D. LaForge, M. M. Qazilbash, A. S. Sefat, D. Mandrus, K. Haule, G. Kotliar, and D. N. Basov, *Phys. Rev. Lett.* **108**, 147002 (2012).
  - <sup>14</sup> A. Georges, L. de' Medici, and J. Mravlje, *Annu. Rev. Condens. Matter Phys.* **4**, 137 (2013).
  - <sup>15</sup> D. Sutter, C. G. Fatuzzo, S. Moser, M. Kim, R. Fittipaldi, A. Vecchione, V. Granata, Y. Sassa, F. Cossalter, G. Gatti, et al., *ArXiv e-prints* (2016), 1610.02854.
  - <sup>16</sup> W. Witczak-Krempa, G. Chen, Y. B. Kim, and L. Balents, *Annual Review of Condensed Matter Physics* **5**, 57 (2014).
  - <sup>17</sup> I. I. Mazin, H. O. Jeschke, K. Foyevtsova, R. Valentí, and D. I. Khomskii, *Phys. Rev. Lett.* **109**, 197201 (2012).
  - <sup>18</sup> K. Foyevtsova, H. O. Jeschke, I. I. Mazin, D. I. Khomskii, and R. Valentí, *Phys. Rev. B* **88**, 035107 (2013).
  - <sup>19</sup> Y. Singh and P. Gegenwart, *Phys. Rev. B* **82**, 064412 (2010).
  - <sup>20</sup> H. Gretarsson, J. P. Clancy, Y. Singh, P. Gegenwart, J. P. Hill, J. Kim, M. H. Upton, A. H. Said, D. Casa, T. Gog, et al., *Phys. Rev. B* **87**, 220407 (2013).
  - <sup>21</sup> S. H. Chun, J.-W. Kim, J. Kim, H. Zheng, C. C. Stoumpos, C. D. Malliakas, J. F. Mitchell, K. Mehlawat, Y. Singh, Y. Choi, et al., *Nat Phys* **11**, 462 (2015).
  - <sup>22</sup> B. H. Kim, G. Khaliullin, and B. I. Min, *Phys. Rev. B* **89**, 081109 (2014).
  - <sup>23</sup> G. Khaliullin, *Phys. Rev. Lett.* **111**, 197201 (2013).
  - <sup>24</sup> A. Akbari and G. Khaliullin, *Phys. Rev. B* **90**, 035137 (2014).
  - <sup>25</sup> O. N. Meetei, W. S. Cole, M. Randeria, and N. Trivedi, *Phys. Rev. B* **91**, 054412 (2015).
  - <sup>26</sup> C. Svoboda, M. Randeria, and N. Trivedi, *Phys. Rev. B* **95**, 014409 (2017).
  - <sup>27</sup> T. Dey, A. Maljuk, D. V. Efremov, O. Kataeva, S. Gass, C. G. F. Blum, F. Steckel, D. Gruner, T. Ritschel, A. U. B. Wolter, et al., *Phys. Rev. B* **93**, 014434 (2016).
  - <sup>28</sup> S. Bhowal, S. Baidya, I. Dasgupta, and T. Saha-Dasgupta, *Phys. Rev. B* **92**, 121113 (2015).
  - <sup>29</sup> G. Cao, T. F. Qi, L. Li, J. Terzic, S. J. Yuan, L. E. DeLong, G. Murthy, and R. K. Kaul, *Phys. Rev. Lett.* **112**, 056402 (2014).
  - <sup>30</sup> G. Chen and L. Balents, *Phys. Rev. B* **84**, 094420 (2011).
  - <sup>31</sup> S. Calder, J. G. Vale, N. A. Bogdanov, X. Liu, C. Donnerer, M. H. Upton, D. Casa, A. H. Said, M. D. Lumsden, Z. Zhao, et al., *Nat. Commun.* **7**, 11651 (2016).
  - <sup>32</sup> G. Jackeli and G. Khaliullin, *Phys. Rev. Lett.* **102**, 017205 (2009).
  - <sup>33</sup> J. c. v. Chaloupka, G. Jackeli, and G. Khaliullin, *Phys. Rev. Lett.* **105**, 027204 (2010).
  - <sup>34</sup> Y. Singh, S. Manni, J. Reuther, T. Berlijn, R. Thomale, W. Ku, S. Trebst, and P. Gegenwart, *Phys. Rev. Lett.* **108**, 127203 (2012).
  - <sup>35</sup> K. A. Modic, T. E. Smidt, I. Kimchi, N. P. Breznay, A. Biffin, S. Choi, R. D. Johnson, R. Coldea, P. Watkins-Curry,

- G. T. McCandless, et al., Nat. Comm. **5**, 4203 (2014).
- <sup>36</sup> T. Takayama, A. Kato, R. Dinnebier, J. Nuss, H. Kono, L. S. I. Veiga, G. Fabbris, D. Haskel, and H. Takagi, Phys. Rev. Lett. **114**, 077202 (2015).
- <sup>37</sup> A. Biffin, R. D. Johnson, I. Kimchi, R. Morris, A. Bombardi, J. G. Analytis, A. Vishwanath, and R. Coldea, Phys. Rev. Lett. **113**, 197201 (2014).
- <sup>38</sup> J. Knolle, G.-W. Chern, D. L. Kovrizhin, R. Moessner, and N. B. Perkins, Phys. Rev. Lett. **113**, 187201 (2014).
- <sup>39</sup> Y. Sizyuk, C. Price, P. Wölfle, and N. B. Perkins, Phys. Rev. B **90**, 155126 (2014).
- <sup>40</sup> I. Kimchi, R. Coldea, and A. Vishwanath, Phys. Rev. B **91**, 245134 (2015).
- <sup>41</sup> Y. Yamaji, Y. Nomura, M. Kurita, R. Arita, and M. Imada, Phys. Rev. Lett. **113**, 107201 (2014).
- <sup>42</sup> K. Pajskr, P. Novák, V. Pokorný, J. Kolorenč, R. Arita, and J. Kuneš, Phys. Rev. B **93**, 035129 (2016).
- <sup>43</sup> K. Oikawa, T. Kamiyama, H. Kato, and Y. Tokura, Journal of the Physical Society of Japan **72**, 1411 (2003).
- <sup>44</sup> H. Kato, T. Okuda, Y. Okimoto, Y. Tomioka, K. Oikawa, T. Kamiyama, and Y. Tokura, Phys. Rev. B **69**, 184412 (2004).
- <sup>45</sup> K. Oikawa, T. Kamiyama, H. Kato, and Y. Tokura, Journal of the Physical Society of Japan **72**, 1411 (2003).
- <sup>46</sup> B. C. Jeon, C. H. Kim, S. J. Moon, W. S. Choi, H. Jeong, Y. S. Lee, J. Yu, C. J. Won, J. H. Jung, N. Hur, et al., Journal of Physics: Condensed Matter **22**, 345602 (2010).
- <sup>47</sup> W. Prellier, V. Smolyaninova, A. Biswas, C. Galley, R. L. Greene, K. Ramesha, and J. Gopalakrishnan, Journal of Physics: Condensed Matter **12**, 965 (2000).
- <sup>48</sup> T. Aharen, J. E. Greedan, C. A. Bridges, A. A. Aczel, J. Rodriguez, G. MacDougall, G. M. Luke, V. K. Michaelis, S. Kroeker, C. R. Wiebe, et al., Phys. Rev. B **81**, 064436 (2010).
- <sup>49</sup> N. Smolentsev, M. Sikora, A. V. Soldatov, K. O. Kvashnina, and P. Glatzel, Phys. Rev. B **84**, 235113 (2011).
- <sup>50</sup> K. Ishii, I. Jarrige, M. Yoshida, K. Ikeuchi, J. Mizuki, K. Ohashi, T. Takayama, J. Matsuno, and H. Takagi, Phys. Rev. B **83**, 115121 (2011).
- <sup>51</sup> We use lower case  $j_{\text{eff}}$  to denote single particle(hole) states, while upper case  $J_{\text{eff}}$  is used for total angular momentum of an ion.
- <sup>52</sup> X. Liu, V. M. Katukuri, L. Hozoi, W.-G. Yin, M. P. M. Dean, M. H. Upton, J. Kim, D. Casa, A. Said, T. Gog, et al., Phys. Rev. Lett. **109**, 157401 (2012).
- <sup>53</sup> L. Hozoi, H. Gretarsson, J. P. Clancy, B.-G. Jeon, B. Lee, K. H. Kim, V. Yushankhai, P. Fulde, D. Casa, T. Gog, et al., Phys. Rev. B **89**, 115111 (2014).
- <sup>54</sup> M. Moretti Sala, K. Ohgushi, A. Al-Zein, Y. Hirata, G. Monaco, and M. Krisch, Phys. Rev. Lett. **112**, 176402 (2014).
- <sup>55</sup> M. Moretti Sala, M. Rossi, S. Boseggia, J. Akimitsu, N. B. Brookes, M. Isobe, M. Minola, H. Okabe, H. M. Rønnow, L. Simonelli, et al., Phys. Rev. B **89**, 121101 (2014).
- <sup>56</sup> K. W. Plumb, A. M. Cook, J. P. Clancy, A. I. Kolesnikov, B. C. Jeon, T. W. Noh, A. Paramakanti, and Y.-J. Kim, Phys. Rev. B **87**, 184412 (2013).
- <sup>57</sup> A. E. Taylor, S. Calder, R. Morrow, H. L. Feng, M. H. Upton, M. D. Lumsden, K. Yamaura, P. M. Woodward, and A. D. Christianson, ArXiv e-prints (2016), 1610.02375.
- <sup>58</sup> D. S. Ellis, J. Kim, J. P. Hill, S. Wakimoto, R. J. Birge-neau, Y. Shvyd'ko, D. Casa, T. Gog, K. Ishii, K. Ikeuchi, et al., Phys. Rev. B **81**, 085124 (2010).